ACS APPLIED NANO MATERIALS

www.acsanm.org Article

Phosphorus Covalent Triazine Framework-Based Nanomaterials for Electrocatalytic Hydrogen Evolution Reaction

Himanshu Sekhar Jena,* Chidharth Krishnaraj, Biraj Kanta Satpathy, Kuber Singh Rawat, Karen Leus, Savita Veerapandian, Rino Morent, Nathalie De Geyter, Veronique Van Speybroeck, Debabrata Pradhan, and Pascal Van Der Voort*

Cite This: https://doi.org/10.1021/acsanm.3c03248 Read Online

ACCESS | Metrics & More | Article Recommendations | Supporting Information

ABSTRACT: The production of hydrogen via electrocatalytic reduction of water using metal-free nanomaterials as the catalyst is a promising and ultimate green approach. Graphitic carbon nitride, covalent organic frameworks, and covalent triazine frameworks (CTFs) are some of the nanostructured materials that are investigated for this purpose. Currently, these materials still lack the efficiency to compete with other techniques (electrolysis). This is because the reaction mechanism and active sites are, in many cases, still poorly understood. In this work, we report a set of metal-free nanostructure-based electrocatalysts, phosphorus covalent triazine frameworks (PCTFs), for electrocatalytic hydrogen production. The hydrogen evolution reaction (HER) performance of PCTF-based nanomaterials is ascribed to the synergistic effect of isolated single nitrogen and phosphorus sites on the large surface area. By combining both experimental and theoretical studies, we found that especially the pyridinic-nitrogen species are the most active sites for the HER. The presence of phosphorus next to the pyridinic-N enhances the HERs. The present results provide a better understanding of the importance of different heteroatoms in nanomaterials as active sites in HERs. Theoretical studies confirmed that phosphorus, being electron rich, creates high electron densities on the nearby N atoms of the CTF materials and intensifies the HER process.

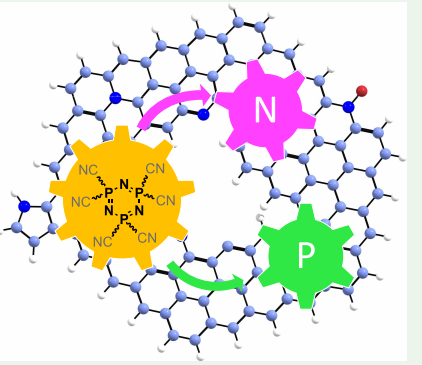

KEYWORDS: *covalent triazine framework, hydrogen evolution reaction, electrocatalysis, porous carbon, single sites, molecular modeling study*

INTRODUCTION

Hydrogen gas is essential to produce ammonia, steel, and aluminum. It also becomes more and more important as a fuel and for methane replacement and in CO_2 transformation process.[1−6] Currently, no less than 96% of H_2 production is based on the reforming of fossil fuels and less than 4% from water electrolysis. The production of H_2 from water is termed the hydrogen evolution reaction (HER). Until now, Pt-based materials are the best electrocatalysts for the HER despite being less abundant and expensive.[7−9] Several other electrocatalysts, e.g., noble metal ions, metal sulfides, phosphides, carbides, borides, metal nanoparticles, and chalcogenides, are reported to potentially replace Pt-based catalysts.[1−6] Much effort has been dedicated to understanding the physical and chemical properties of the active sites of non-Pt-based electrocatalysts.[10] Research has shown that lowering the size of metal-based catalysts from bulk to nanoparticles and from clusters to single atom/site increases the performance of the materials.[11] Nonmetallic heteroatoms (N, P, and S)-doped nanostructured carbons are particularly attractive as they can be synthesized with a large surface area at low cost and have a high stability and tunable conductivities.[12,13] These nanomaterials can also be used as support to anchor transition metal ion-based single-atom catalysts or, preferably, be used as a metal-free electrocatalyst for the HER.[14−18]

It has been demonstrated that engineering carbon-based nanoporous materials by doping phosphorus greatly enhances the HER performance. Until now, postsynthetic incorporation (called as chemical doping) using melamine, urea/pyrrole for N and triphenylphosphine/phytic acid for P is the only method reported so far.[19−22] However, by this method, it is difficult to ensure the location of the heteroatoms and their environments, random incorporation of heteroatoms, doping level, configuration of chemical bonding, and most importantly their reproducibility. This makes it more difficult to understand any possible synergistic effects between two or more active sites and distinguish the role of each in catalysis.

Received: July 14, 2023
Revised: November 10, 2023
Accepted: November 12, 2023

Scheme 1. Schematic Representation of (a) Ideal PCTF, (b) PCTF Synthesized under Ionothermal Conditions Showing Possible Locations of Different Types of N and P Sites, and (c) Four Different Types of N-Species Formed after the Ionothermal Synthesis Characterized from XPS Analysis

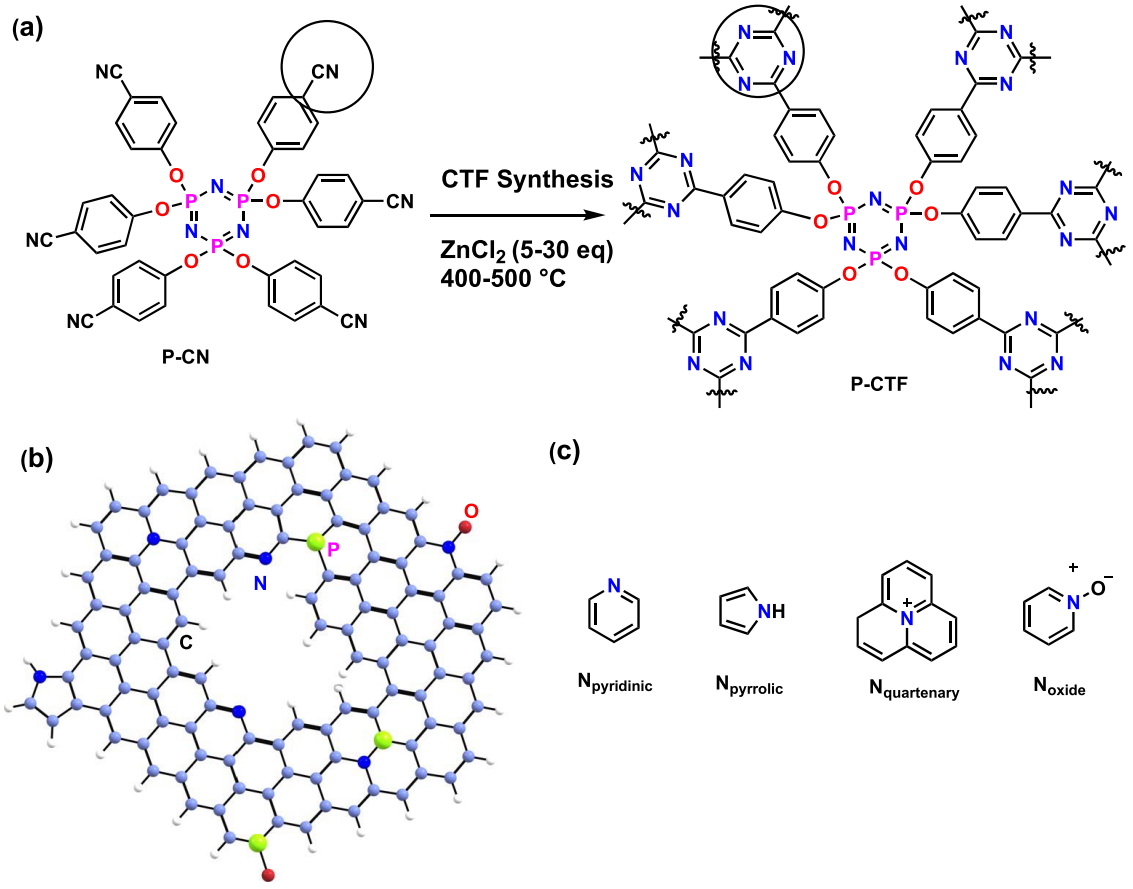

Among carbon-based nanoporous materials, covalent triazine frameworks (CTFs) are promising nanomaterials in electrocatalysis.[23−25] CTFs are considered as highly chemically stable porous N-rich materials with many potential applications. CTF materials are generally prepared under ionothermal (using molten $ZnCl_2$) and solvothermal conditions.[26−31] (see Scheme 1 for an example). The CTFs are formed in a 2D porous system by $\pi-\pi$ stacking (typically an AA stacking) of individual flat polymer sheets, as in graphite. The CTF-based materials obtained through ionothermal conditions have been studied in gas separation, heterogeneous catalysis, and electrocatalysis because of the presence of defects based on different N-species formed during ionothermal synthesis.[26,32,33]

In the past few years, CTF materials have been engineered to better understand their properties and to improve their importance in certain applications. It starts with the design and synthesis of new building units containing novel functionalities or leading to new topologies or porosities. Particularly, (i) CTFs with enhanced N-species and enhanced hydrophobicity (high F-content) are developed to improve their CO_2 adsorption and separation from mixture of gases;[32−36] (ii) pyridine-, bipyridine-, acetylacetone-, 1,4,5,8,9,12-hexaazatriphenylen-, and N-heterocyclic carbene-based CTFs have been developed for a wide range of heterogeneous catalytic reactions;[26,33,37−39] (iii) donor−acceptor (D−A) type CTFs with alternating electron-donating and -accepting groups have been created for photocatalytic applications;[40−42] and (iv) noble and non-noble metal-based catalysts supported by CTF have been developed for electrocatalysis.[23,39,43]

Recently, we have explored the effect of different defect N-species for the HER and oxygen reduction reaction.[43] We and several other groups reported that pyridinic-N and quaternary-Ns are the most favorable sites for water and oxygen interactions for electrocatalysis.[17,18,44,45] Metal-free CTFs and covalent organic frameworks (COFs) obtained from mild synthesis condition have been recently reported as photocatalysts for hydrogen generation.[23,40,41,46−48] Similar to doped graphene, g-C_3N_4, and porous carbon, it is expected that CTFs containing phosphorus atoms might be more active than pristine CTFs in electrocatalysis.[18,22] However, this type of CTF-based material is not yet explored as an electrocatalyst.

In this work, we used hexakis-(4-cyanophenyloxy)-cyclotriphosphazenes (P-CN) as a linker to synthesize four different phosphorus CTFs (PCTFs) under different ionothermal conditions. The four CTFs have varying amounts and types of N- and P- species. To explore the synergistic role of N and P in electrocatalysis, all four CTFs were used as electrocatalysts for the HER. Using both experiments and theoretical modeling, we explored the synergistic effect of N and P sites for the hydrogen production.

RESULTS AND DISCUSSION

Synthesis of PCTFs. We use a dinitrile building unit containing phosphazene core. Under the ionothermal synthesis, by varying the $ZnCl_2$ amount (5, 10, and 30

https://doi.org/10.1021/acsanm.3c03248
ACS Appl. Nano Mater. XXXX, XXX, XXX−XXX

Table 1. BET Surface areas, Pore Volumes, Elemental Composition, Relative Number of N-Species, CO_2 Uptake, and CO_2/N_2 Selectivity of the Presented PCTFs.

						relative number of N-species (at %)[d]				relative number of P-species (at %)[d]		
materials	SA_{BET}[a] (m^2/g)	V_t[b] (cm^3/g)	N (%)[c]	N (%)[d]	P (%)[d]	$N_{Pyridinic}$	$N_{Pyrrolic}$	$N_{Quaternary}$	$N_{oxidized}$	C−P	N−P	P−O
PCTF-10400	1159	0.55	8.72	6.99	1.84	36	29	24	10	23	57	20
PCTF-5500	1316	0.62	8.07	6.78	1.33	28	43	14	5	13	60	27
PCTF-10500	1407	0.83	7.84	6.68	0.68	36	27	28	9	20	64	16
PCTF-30500	2027	1.32	6.90	6.11	0.63	33	33	23	11	17	58	25

[a]BET surface area was calculated over the relative pressure range of 0.01−0.05 at 77 K. [b]V_t, total pore volume was calculated at P/P_0 = 0.98. [c]Percentage of carbon and nitrogen content calculated from elemental analysis [d]Relative amount of each N-species in atomic percent (at %) calculated from XPS analysis (the values in the parentheses correspond to their binding energies in eV).

equivalents) at two different temperatures (400 and 500 °C), four different PCTF-based materials were synthesized (Scheme 1). For clarity, the four PCTFs are referred to as PCTF-xy where x is the $ZnCl_2$ equivalent and y is the synthesis temperature (Tables 1 and S1). Synthesis of CTF with a uniform distribution of heteroatoms created an electron delocalization on the extended 2D sheet structure, facilitating activation and conversion of water molecules to molecular hydrogen. Furthermore, the π-stacking interactions between the CTF layers and the larger surface area enable the facile diffusion of water molecules into the pore and interaction with the electron-rich active sites.

Characterization of PCTFs. For the preliminary characterization of the four PCTFs, FT-IR measurements were performed to confirm the complete trimerization of the nitrile group to a triazine ring (Figure 1). In the case of the linker P-

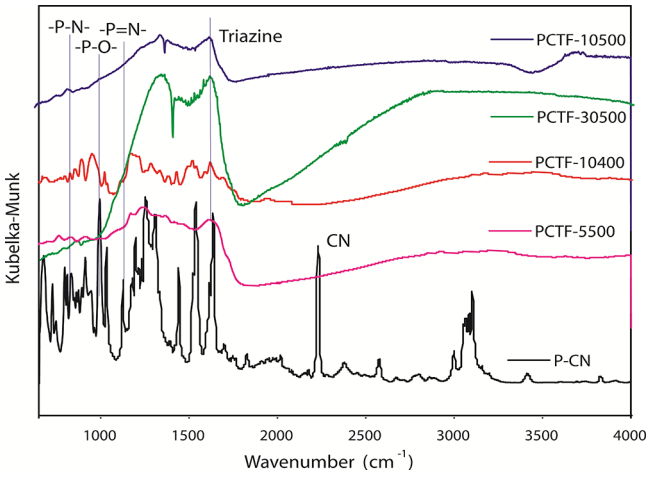

Figure 1. DRIFTs FT-IR spectra of P-CN and PCTFs.

CN, the CN band at 2230 cm^{-1}, the −P═N− bands between 1290 and 1180 cm^{-1}, the −P−O−C− bands between 1150 and 982 cm^{-1}, and the −P−N− band at 900 cm^{-1} are compared with the PCTFs. After the ionothermal synthesis, the absence of the −CN band at 2230 cm^{-1} and the presence of a −C═N (triazine) band at 1598 and 1388 cm^{-1} confirmed the complete conversion of the nitrile groups to triazine rings. Additional peaks at 1162, 783, and 938 cm^{-1} confirmed the presence of the phosphazene core unit and −P−O− groups.[49,50] The elemental analysis (Table 1) confirmed a significant amount of Ns (8.72−6.90 wt%) in the four materials. It is known that during the ionothermal synthesis, heteroatoms combine and release as molecular gas (N_2), and therefore the N content in the final CTF material is generally lower than in the building units.

The chemical composition, functionalities, and respective binding energy were further characterized by XPS measurements. The amount of each element is again determined from the XPS analysis and corresponds well to the CHNS analysis (Table 1). This observation suggests that the amount of $ZnCl_2$ and the synthesis temperature influence the number of heteroatoms (N and P) in the final PCTF materials. The amount of N (6.99−6.11 wt%) and P (1.84−0.63 wt%) in all four PCTFs are comparable to a similar set of P-N-doped porous materials.[21,22,34,51] In order to gain more information on the functional groups and their local environments, XPS spectra of all PCTFs were analyzed by fitting the respective species to their binding energies.[52] The C1s spectra of all PCTFs featured the characteristic peaks for aromatic C−C/C═C and triazine C═N/C−N species at 284.8 and 286 eV, respectively (Figure S1). The deconvoluted N 1s and P2p spectra of all PCTFs are shown in Figure 2, and the relative atomic % is given in Table 1. All samples showed four different peaks that correspond to four different types of N-species, pyridinic-N (N_{py}), pyrrolic-N (N_{pyr}), quaternary-N (N_{qu}), and pyridinic-N-oxide (N_{ox}), at 398.7, 400.1, 401.4, and 402.9 eV, respectively (Figure 2 left, Scheme 1b). The relative amount of each N-species is calculated by considering the area under each fitted curve and included in Table 1. The four set of N-species are very commonly observed in CTF-based materials synthesized under ionothermal conditions.[52] Except PCTF-5500, three other PCTF materials contain very similar amounts of different N-species. Importantly, PCTF-5500 contains a greater amount of pyrrolic-N than others. In addition, the P2p1/2 spectra of all four PCTFs showed peaks at 133.2, 134.3, and 135.5 eV that can be assigned to P−C, P−N, and P−O species, respectively (Figure 2 right, Scheme 1b).

Powder X-ray diffraction (PXRD) measurements of all PCTFs were carried out at room temperature (Figure S2). The PXRD patterns show a broad peak in the range 2θ = 20−30°. This feature is well corroborated with most CTF-based materials under ionothermal conditions. The broad peak can be attributed to the pre-existing layered structures or subsequent graphitization of the materials during pyrolysis.[31,29] From the thermogravimetric analysis, it is confirmed that all of the PCTFs are equally stable like other CTF-based materials until 500 °C (Figure S3). PCTF-10400 decomposes earlier than the other three materials synthesized at 500 °C.

Gas Sorption Properties. The surface properties of all of the PCTF materials were evaluated using N_2 sorption measurements at 77 K (Figure 3). All materials were activated overnight under vacuum at 150 °C before the analysis. The

https://doi.org/10.1021/acsanm.3c03248
ACS Appl. Nano Mater. XXXX, XXX, XXX−XXX

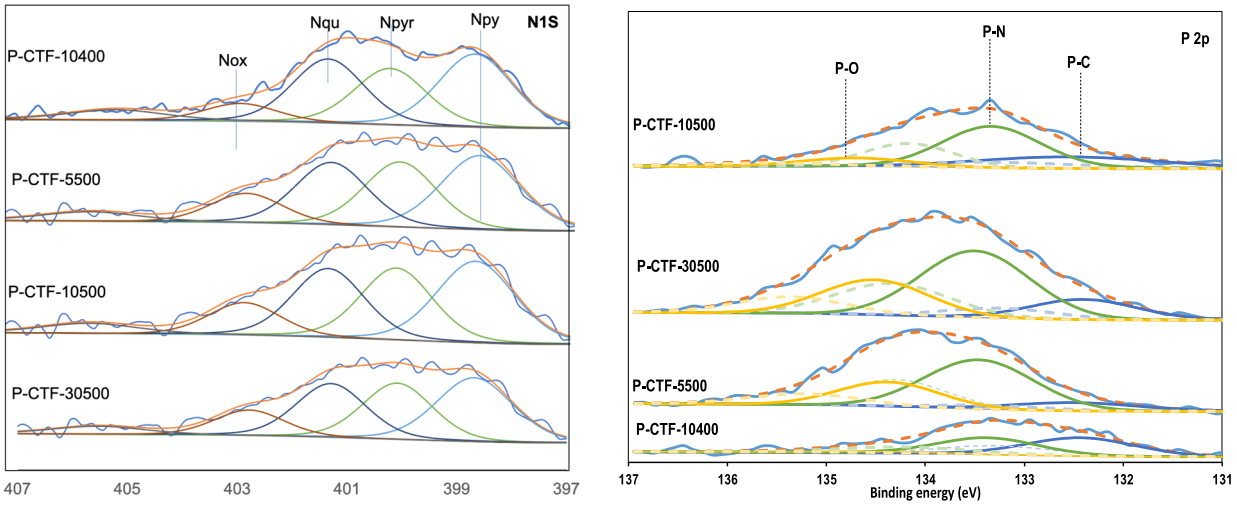

Figure 2. Deconvolution of the N 1s (left) and P 2p (right) XPS spectrum of PCTFs and possible different N- and P-species formed during ionothermal synthesis.[23,52]

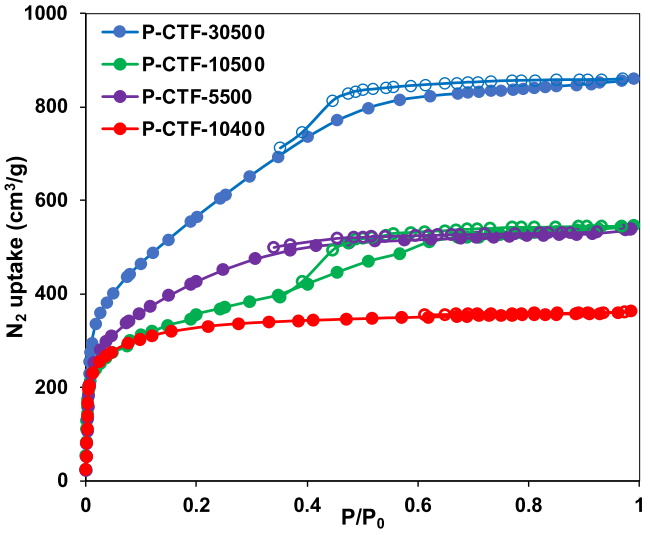

Figure 3. Nitrogen adsorption/desorption isotherms of PCTFs measured at 77 K; filled and empty symbols represent, respectively, adsorption and desorption.

surface areas and total pore volumes (V_t), calculated at P/P_0= 0.98 for all PCTFs are included in Table 1. On comparison, it was found that PCTF-30500 that was synthesized using 30 equiv of $ZnCl_2$ at 500 °C exhibited the highest surface area of 2027m^2/g and a total pore volume of 1.32 cm^3/g. It is important to note that in all four PCTF materials, a sharp increase of N_2 uptake at relatively low pressure (<0.01) confirmed the presence of micropores.[32,33,43] In addition, PCTF-10500 and PCTF-30500 showed hysteresis between the adsorption and desorption isotherms between 0.4 and 0.9 relative pressure. A similar observation was noticed in CTF-based materials synthesized at higher temperatures and is ascribed to the formation of narrow and slit-shaped pores that strongly interact with N_2.[34]

The analysis of the materials confirmed that all four PCTF materials are thermally robust, have a large surface area and pore volume, and contain P and N heteroatoms with different oxidation states and functionalities. The electrocatalytic performance of these PCTFs was further explored in the electrocatalytic HER.

Electrochemical HER. All catalysts were further evaluated as HER electrocatalysts in an N_2-saturated 0.5 H_2SO_4 electrolyte. Figure 4a shows the linear sweep voltammetry (LSV) plots of all of the PCTFs along with standard Pt/C for comparison. The HER current is found to increase differently as the potential scanned negative for the different samples. A rapid increase in the reduction current is found for PCTF-10500 compared to the other PCTFs. This suggests PCTF-10500 is more active for hydrogen production than the other three PCTFs. The onset potential for HER is measured from the intercept potential by taking the tangents from the fast-rising current portion to the baseline current portion. The effectiveness of an HER catalyst is normally known from the overpotential required to achieve 10 mA/cm^2. The onset potential and overpotential for different samples are listed in Table 2. Among the PCTFs, PCTF-10500 shows the lowest overpotential of 227 mV indicating its superiority over the other PCTFs. The overpotential value of PCTFs is comparable with the similar sort of heteroatom-doped porous material (Table S2) and especially better than metal-free COF-based electrocatalysts, g-C_3N_4 type of materials, and microporous graphitic frameworks.[34,53−59]

Moreover, to study the HER kinetics of the prepared samples, the overpotential versus log *i*, also called the Tafel plot, is plotted as shown in Figure 4b. The Tafel slope suggests the reaction kinetics at the electrode surface. The lower the Tafel slope, the better the electrochemical kinetics at the electrode surface. The smallest Tafel slope value from PCTF-10500 suggests its higher HER activity (Table 2). The electrochemical surface area (ECSA) is further evaluated from the double-layer capacitances obtained in the non-Faradaic region (−0.05 to −0.15 V) of cyclic voltammetry (CV) at different scan rates using the relation ECSA = C_{dl}/C_s, where C_{dl} is the electrochemical double-layer capacitance and C_s is the specific electrochemical double layer capacitance of an atomically smooth surface (taken here as 40 μF cm^{-2}). From the obtained CV profiles (Figure S4), the current measured at −0.14 V is plotted against the scan rates (Figure 4c) to determine the C_{dl} values. The slope of the almost straight line is used to measure the respective C_{dl} values for the ECSA calculation. The calculated C_{dl} and ECSA values for the sample PCTF-10500 are found to be 87 μF and 2.175 cm^2,

https://doi.org/10.1021/acsanm.3c03248
ACS Appl. Nano Mater. XXXX, XXX, XXX−XXX

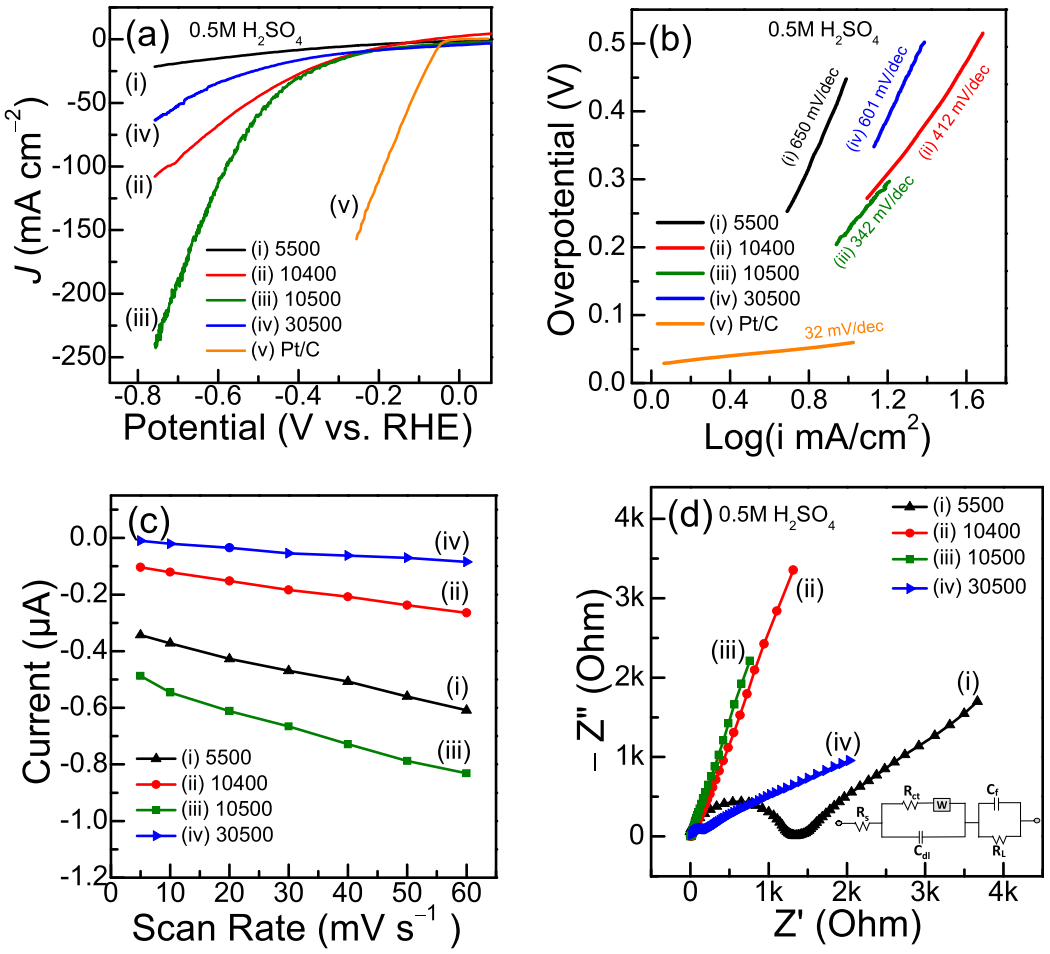

Figure 4. (a) LSV profiles at 20 mV s^{-1}, (b) corresponding Tafel plots, (c) current versus scan rate, and (d) Nyquist plots of different samples. All of the electrochemical measurements were performed in 0.5 M H_2SO_4 solution.

Table 2. HER Performance of PCTFs

sample	onset potential (mV)	overpotential (mV)@10 mA cm^{-2}	tafelslope (mV dec^{-1})	C_{dl} (μF)	ECSA (cm^2)	R_{ct} (Ω)
PCTF-5500	210	456	650	70.21	1.75	490
PCTF-10400	129	244	412	41	1.025	35.03
PCTF-10500	114	227	342	87	2.175	11.6
PCTF-30500	139	255	601	13.25	0.331	390.3
Pt/C	38	59	32			

respectively, which are higher than those for the other PCTFs. This suggests the presence of more electrochemically active sites in PCTF-10500 and hence exhibiting better HER activity.

The EIS analysis was performed to determine the charge-transfer resistance (R_{ct}). The diameter of the semicircle in the high-frequency region of Nyquist plots (Figure 4d) is used to determine the R_{ct} value, whereas the straight line in the low-frequency region corresponds to the diffusion of ions at the working electrode. The obtained Nyquist plots for the PCTFs are fitted with an equivalent circuit with different elements such as solution resistance (R_s), R_{ct}, constant phase element, Warburg impedance element (W), and leakage resistance (R_L) as shown in the inset of Figure 4d. The measured R_{ct} value is found to be the lowest (11.6 Ω) for PCTF-10500 (Table 2), suggesting higher charge transfer at the electrode/electrolyte interface. Moreover, the straight line in the lower-frequency region has a higher slope for PCTF-10500 than other samples, indicating its ease in the diffusion process.

On comparison, among all four CTF materials, we found that the HER activity followed the order PCTF-10500 > PCTF-10400 > PCTF-30500 > PCTF-5500. The obtained electrocatalytic test results unambiguously point to PCTF-10500 as the best metal-free electrocatalyst among other PCTFs and P-doped porous materials. Among PCTFs, PCTF-10500 contains a higher amount of electrochemically active N-sites and shows better diffusion and higher charge transfer at the electrode/electrolyte surface. The HER performance is further correlated with the physical and chemical properties of the PCTFs. We found that the surface area, the pore volume, and the number of heteroatoms of PCTF-10500 are very close to those of other PCTFs. The combination of number of N_{py} and N_{qu} sites is higher than in the other three PCTFs. We also compared the P content in the four PCTFs with respect to HER activity. We found that PCTF-10500 (0.68 wt%) and PCTF-10400 (1.84 wt %), though the amount of P is significantly different from one other, had better HER activity

https://doi.org/10.1021/acsanm.3c03248
ACS Appl. Nano Mater. XXXX, XXX, XXX−XXX

than the other two CTFs with a similar range of P contents. In addition, the uniform distribution of N and P sites onto the CTF influences the local electronic structure, and therefore the most electron rich centers act as improved catalytic sites for electrocatalytic reactions.[60] To further explore the benefits of heteroatoms, we performed an in-depth theoretical modeling by considering the position of heteroatoms and their environment.

A computational study is further performed on various models of PCTF-based catalysts to understand the role of different N-species and P toward the HER activity. All calculations are executed at the PBE-D3(BJ)[61−63] level of theory using VASP[64,65] (more details are in the SI). Experimental results suggest that all PCTFs comprise four types of N-species with P. However, the catalyst with higher N_{py} and N_{qu} sites (PCTF-10500) shows the best HER activity. Therefore, we have strategically studied the possible arrangements of N_{py}, N_{qu}, and P sites in the PCTF-based catalysts with fixed positions of N_{ox} and N_{pyr}. Various positions of N_{py} are considered using an initial structure (Figure S5). After finding the preferable site for N_{py}, the combinations of N_{qu} and P are also investigated, keeping the position of N_{py} fixed (Figures S6−S9).

Out of all possible cases, the four most stable arrangements of active sites and their environment (Figure 5) are used for

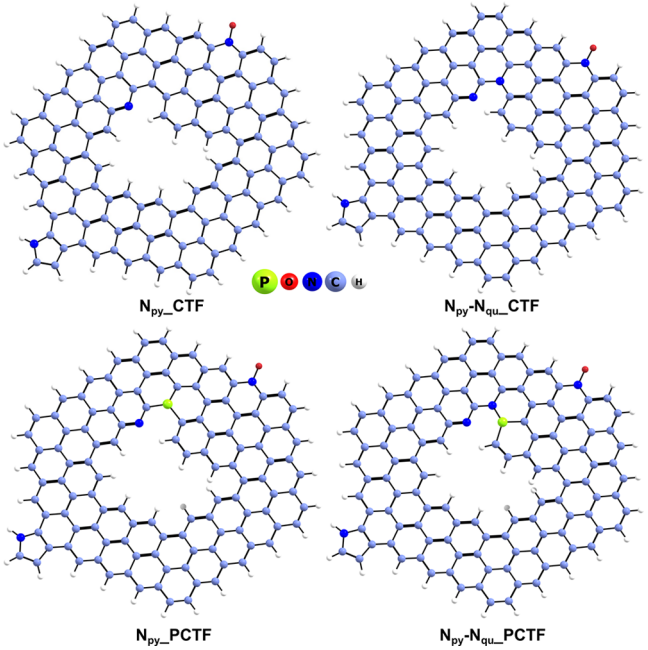

Figure 5. Optimized structures of possible active units of the PCTFs based on different arrangements of nitrogen and phosphorus sites.

the further calculation of HER. These four cases are N_{py}_CTF (with N_{py}), N_{py}-N_{qu}_CTF (combination of N_{py} and N_{qu}), N_{py}_PCTF (combination of N_{py} and P), and N_{py}-N_{qu}_PCTF (combination of N_{py}, N_{qu} and P). The thermodynamic stability of the most stable structures is also assessed through their formation (Table S3) and binding energy (more details in the SI).

In general, the HER process completes in two steps; the first step is H adsorption (H*; where * is the catalyst), referred as the Volmer step, which is followed by the desorption of H* in the second step, named the Heyrovsky step or the Tafel step.[21,22,61,62] As the free energy of H* provides a good descriptor for the catalytic activity of HER, we have calculated the free energy of H* ($H^+ + e^- + * \rightarrow H^*$;) for each modeled system using the computational hydrogen electrode model[66] at a potential of U = 0 relative to the standard hydrogen electrode (Figure 6). An ideal HER catalyst should have zero free energy

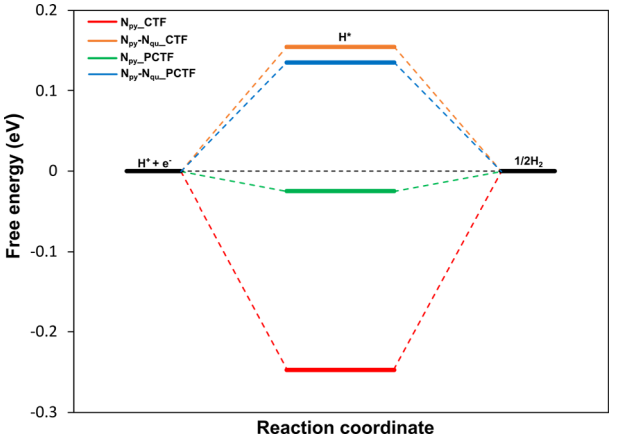

Figure 6. Calculated free-energy diagram for HER at 0 V.

of H*.[25] The calculated free energies for N_{py}_CTF and N_{py}-N_{qu}_CTF are −0.25 and 0.15 eV at the N_{py} site. Here, the combination of N_{py} and N_{qu} shows better HER activity than only N_{py}. We also considered H* at the N_{qu} site on N_{py}-N_{qu}-CTF, and the free energy for H* is calculated as 1.80 eV (Figure S10). This suggests that N_{py} is a more active site for HER than N_{qu} as H atom absorption becomes difficult to achieve at N_{qu}. Therefore, only the N_{py} site is further explored to evaluate the HER activity on other PCTFs. Moreover, the addition of a P atom near N_{py} (N_{py}_PCTF) has a crucial effect on favoring the HER activity (−0.03 eV) via destabilizing the formation of H* compared to pristine N_{py}_CTF in which overall HER is not favorable as N_{py}_CTF is quite favorable for H* formation but not for overall HER as the hydrogen atom binds quite strongly. The calculated free energy of H* is 0.14 eV for N_{py}-N_{qu}_PCTF, which also identifies as a better candidate for overall HER than N_{py}_CTF. The calculated free-energy diagram reveals that the presence of N_{qu} and P atoms near N_{py} improves the HER activity compared to pristine N_{py}, and N_{py}_PCTF identifies as a best candidate among all.

CONCLUSIONS

In this study, a new set of PCT- based nanomaterials were synthesized using the dinitrile monomer containing the phosphazene core and explored as electrocatalysts for HER. The HER study revealed that PCTF that was obtained by using 10 equiv of $ZnCl_2$ at 500 °C is the best HER catalyst. The HER performance in terms of overpotential is further found to be comparable to other heteroatom-doped porous nanostructured materials and is better than those of g-C_3N_4, COFs, and microporous graphitic carbon frameworks. Using both experimental evidence and molecular modeling, we conclude that the uniform distribution of the active species over the large surface area is necessary for enhanced activity. The number of heteroatoms as active sites and the neighboring carbons are equally important to understand the electrocatalytic performance. Among the different N-species in N-doped porous nanomaterials, pyridinic-N is more active than

https://doi.org/10.1021/acsanm.3c03248
ACS Appl. Nano Mater. XXXX, XXX, XXX−XXX

others. The presence of phosphorus in N-rich porous materials creates a high electron density on the nearby carbon atoms which subsequently actually act as the active sites instead of P itself, consequently enhancing the overall electrochemical activity. Moreover, these CTF-based materials with a large surface area have the potential to be used as efficient electrocatalysts by tuning the nature, number, and distribution of heteroatoms, defects, and configuration of chemical bonding around the heteroatoms.

MATERIALS AND METHODS

The required chemicals were purchased from Sigma-Aldrich and used without further purifications. The linker, P-CN, was synthesized using the reported literature[50] and was used in CTF synthesis following our previous works.[32,33] Elemental analyses were carried out on a Thermo Scientific Flash 2000 CHNS-O analyzer equipped with a TCD detector. FT-IR spectroscopy in the region of 4000−650 cm^{-1} was performed with a Thermo Nicolet 6700 FT-IR spectrometer equipped with a nitrogen-cooled MCT detector and a KBr beam splitter. Dinitrogen (N_2) adsorption isotherms were obtained using a Belsorp Mini apparatus measured at 77 K. PXRD patterns were collected on a Thermo Scientific ARL X'Tra diffractometer operated at 40 kV and 30 mA using Cu-K_α radiation (λ = 1.5406 Å). Thermogravimetric analyses (TGAs) were performed on a Netzsch STA-449 F3 Jupiter-simultaneous TG-DSC analyzer in the temperature range of 20-800 °C under a N_2 atmosphere and a heating rate of 2 °C /min. XPS measurements were performed on a Thermo Fisher Scientific K-Alpha. All electrochemical measurements were performed in a conventional three-electrode system using a CHI 760D electrochemical workstation. Modified rotating disk electrode (RDE), Pt wire, and saturated calomel electrode were used here as the working, counter, and reference electrodes, respectively. The modified RDE was prepared by drop-casting slurry of the synthesized electrocatalyst material on the precleaned RDE electrode. The slurry was prepared by ultrasonically dispersing 5 mg of the electrocatalyst in 1 mL of isopropanol with 20 μL of 5% Nafion solution for 1 h. 80 μL of slurry was drop-casted on the RDE.

ASSOCIATED CONTENT

Supporting Information

The Supporting Information is available free of charge at https://pubs.acs.org/doi/10.1021/acsanm.3c03248.

Detailed experimental procedure with Table, C1s XPS analysis, PXRD analysis, TGA, and computational details (PDF)

Final coordinates of atoms in all relevant structures for free-energy calculations (ZIP)

AUTHOR INFORMATION

Corresponding Authors

Himanshu Sekhar Jena − *Center for Ordered Materials, Organometallics and Catalysis (COMOC), Department of Chemistry, Ghent University, 9000 Ghent, Belgium;* orcid.org/0000-0002-5869-5226; Email: hsjena@gmail.com

Pascal Van Der Voort − *Center for Ordered Materials, Organometallics and Catalysis (COMOC), Department of Chemistry, Ghent University, 9000 Ghent, Belgium;* orcid.org/0000-0002-1248-479X; Email: Pascal.VanDerVoort@UGent.be

Authors

Chidharth Krishnaraj − *Center for Ordered Materials, Organometallics and Catalysis (COMOC), Department of Chemistry, Ghent University, 9000 Ghent, Belgium*

Biraj Kanta Satpathy − *School of Nanoscience and Technology, Materials Science Centre, Indian Institute of Technology Kharagpur, Kharagpur, West Bengal 721 302, India;* orcid.org/0000-0002-7639-024X

Kuber Singh Rawat − *Center for Molecular Modeling (CMM), Ghent University, B-9052 Zwijnaarde, Belgium*

Karen Leus − *Faculty of Engineering and Architecture, Department of Applied Physics, Ghent University, 9000 Ghent, Belgium*

Savita Veerapandian − *Faculty of Engineering and Architecture, Department of Applied Physics, Ghent University, 9000 Ghent, Belgium*

Rino Morent − *Faculty of Engineering and Architecture, Department of Applied Physics, Ghent University, 9000 Ghent, Belgium*

Nathalie De Geyter − *Faculty of Engineering and Architecture, Department of Applied Physics, Ghent University, 9000 Ghent, Belgium*

Veronique Van Speybroeck − *Center for Molecular Modeling (CMM), Ghent University, B-9052 Zwijnaarde, Belgium;* orcid.org/0000-0003-2206-178X

Debabrata Pradhan − *School of Nanoscience and Technology, Materials Science Centre, Indian Institute of Technology Kharagpur, Kharagpur, West Bengal 721 302, India;* orcid.org/0000-0003-3968-9610

Complete contact information is available at: https://pubs.acs.org/10.1021/acsanm.3c03248

Author Contributions

The manuscript was written through contributions of all authors. All authors have given approval to the final version of the manuscript. All scheme and figure images that appear in the manuscript and Supporting Information files (where applicable), including those in the TOC graphic, were original (not published previously or downloaded from the Internet) and created by the authors of this manuscript.

Notes

The authors declare no competing financial interest.

ACKNOWLEDGMENTS

H.S.J., C.K., and P.V.D.V. acknowledge the Research Board of Ghent University (GOA010-17, BOF GOA2017000303) for the support. D.P. acknowledges the SERB (EMR/2017/000697) for funding. The computational resources (Stevin Supercomputer Infrastructure) and services used in this work were provided by the VSC (Flemish Supercomputer Center) and funded by the Ghent University, FWO and the Flemish Government−department EWI.

ABBREVIATIONS

CTF	Covalent Triazine Framework
HER	Hydrogen Evolution Reaction
COFs	Covalent Organic Framework
XPS	X-ray Photoelectron Spectroscopy
NMR	Nuclear Magnetic Resonance
FT-IR	Fourier-transform infrared spectroscopy.

REFERENCES

(1) Hu, C. G.; Dai, L. M. Carbon-Based Metal-Free Catalysts for Electrocatalysis beyond the ORR. *Angewandte Chemie-International Edition* **2016**, *55* (39), 11736−11758.

(2) Siwal, S. S.; Yang, W. Q.; Zhang, Q. B. Recent progress of precious-metal-free electrocatalysts for efficient water oxidation in acidic media. *Journal of Energy Chemistry* **2020**, *51*, 113−133.
(3) Yang, D. H.; Tao, Y.; Ding, X. S.; Han, B. H. Porous organic polymers for electrocatalysis. *Chemical Society Reviews* **2022**, *51* (2), 761−791.
(4) Zhang, J.; Chen, G. B.; Mullen, K.; Feng, X. L. Carbon-Rich Nanomaterials: Fascinating Hydrogen and Oxygen Electrocatalysts. *Adv. Mater.* **2018**, *30* (40), No. 1800528.
(5) Chen, H.; Liang, X.; Liu, Y. P.; Ai, X.; Asefa, T.; Zou, X. X. Active Site Engineering in Porous Electrocatalysts. *Adv. Mater.* **2020**, *32* (44), No. 2002435.
(6) Hu, C. G.; Paul, R.; Dai, Q. B.; Dai, L. M. Carbon-based metal-free electrocatalysts: from oxygen reduction to multifunctional electrocatalysis. *Chemical Society Reviews* **2021**, *50* (21), 11785.
(7) Cheng, N.; Stambula, S.; Wang, D.; Banis, M. N.; Liu, J.; Riese, A.; Xiao, B.; Li, R.; Sham, T. K.; Liu, L. M.; Botton, G. A.; Sun, X. Platinum single-atom and cluster catalysis of the hydrogen evolution reaction. *Nat. Commun.* **2016**, *7*, 13638.
(8) Yin, X.-P.; Wang, H.-J.; Tang, S.-F.; Lu, X.-L.; Shu, M.; Si, R.; Lu, T.-B. Engineering the Coordination Environment of Single-Atom Platinum Anchored on Graphdiyne for Optimizing Electrocatalytic Hydrogen Evolution. *Angewandte Chemie International Edition* **2018**, *57* (30), 9382−9386.
(9) Liu, D.; Li, X.; Chen, S.; Yan, H.; Wang, C.; Wu, C.; Haleem, Y. A.; Duan, S.; Lu, J.; Ge, B.; Ajayan, P. M.; Luo, Y.; Jiang, J.; Song, L. Atomically dispersed platinum supported on curved carbon supports for efficient electrocatalytic hydrogen evolution. *Nature Energy* **2019**, *4* (6), 512−518.
(10) Dubouis, N.; Grimaud, A. The hydrogen evolution reaction: from material to interfacial descriptors. *Chemical Science* **2019**, *10* (40), 9165−9181.
(11) Xiao, Z. H.; Xie, C.; Wang, Y. Y.; Chen, R.; Wang, S. Y. Recent advances in defect electrocatalysts: Preparation and characterization. *Journal of Energy Chemistry* **2021**, *53*, 208−225.
(12) Rahman, M. Z.; Davey, K.; Qiao, S.-Z. Carbon, nitrogen and phosphorus containing metal-free photocatalysts for hydrogen production: progress and challenges. *Journal of Materials Chemistry A* **2018**, *6* (4), 1305−1322.
(13) Rahman, M. Z.; Kibria, M. G.; Mullins, C. B. Metal-free photocatalysts for hydrogen evolution. *Chemical Society Reviews* **2020**, *49* (6), 1887−1931.
(14) Choi, C. H.; Kim, M.; Kwon, H. C.; Cho, S. J.; Yun, S.; Kim, H.-T.; Mayrhofer, K. J. J.; Kim, H.; Choi, M. Tuning selectivity of electrochemical reactions by atomically dispersed platinum catalyst. *Nat. Commun.* **2016**, *7* (1), 10922.
(15) Zhang, H.; An, P.; Zhou, W.; Guan, B. Y.; Zhang, P.; Dong, J.; Lou, X. W. Dynamic traction of lattice-confined platinum atoms into mesoporous carbon matrix for hydrogen evolution reaction. *Science. Advances* **2018**, *4* (1), No. eaao6657.
(16) Shalom, M.; Gimenez, S.; Schipper, F.; Herraiz-Cardona, I.; Bisquert, J.; Antonietti, M. Controlled Carbon Nitride Growth on Surfaces for Hydrogen Evolution Electrodes. *Angewandte Chemie International Edition* **2014**, *53* (14), 3654−3658.
(17) Peng, Z.; Yang, S.; Jia, D.; Da, P.; He, P.; Al-Enizi, A. M.; Ding, G.; Xie, X.; Zheng, G. Homologous metal-free electrocatalysts grown on three-dimensional carbon networks for overall water splitting in acidic and alkaline media. *Journal of Materials Chemistry A* **2016**, *4* (33), 12878−12883.
(18) Zhang, B.; Wang, H.-H.; Su, H.; Lv, L.-B.; Zhao, T.-J.; Ge, J.-M.; Wei, X.; Wang, K.-X.; Li, X.-H.; Chen, J.-S. Nitrogen-doped graphene microtubes with opened inner voids: Highly efficient metal-free electrocatalysts for alkaline hydrogen evolution reaction. *Nano Research* **2016**, *9* (9), 2606−2615.
(19) Zheng, Y.; Jiao, Y.; Li, L. H.; Xing, T.; Chen, Y.; Jaroniec, M.; Qiao, S. Z. Toward Design of Synergistically Active Carbon-Based Catalysts for Electrocatalytic Hydrogen Evolution. *ACS Nano* **2014**, *8* (5), 5290−5296.
(20) Sun, Y.-N.; Zhang, M.-L.; Zhao, L.; Sui, Z.-Y.; Sun, Z.-Y.; Han, B.-H. A N, P Dual-Doped Carbon with High Porosity as an Advanced Metal-Free Oxygen Reduction Catalyst. *Adv. Mater. Interfaces* **2019**, *6* (14), No. 1900592.
(21) Liu, Z.; Ai, J.; Sun, M.; Han, F.; Li, Z.; Peng, Q.; Wang, Q.-D.; Liu, J.; Liu, L. Phosphorous-Doped Graphite Layers with Outstanding Electrocatalytic Activities for the Oxygen and Hydrogen Evolution Reactions in Water Electrolysis. *Adv. Funct. Mater.* **2020**, *30* (12), No. 1910741.
(22) Kumatani, A.; Miura, C.; Kuramochi, H.; Ohto, T.; Wakisaka, M.; Nagata, Y.; Ida, H.; Takahashi, Y.; Hu, K.; Jeong, S.; Fujita, J.-i.; Matsue, T.; Ito, Y. Chemical Dopants on Edge of Holey Graphene Accelerate Electrochemical Hydrogen Evolution Reaction. *Adv. Sci.* **2019**, *6* (10), No. 1900119.
(23) Lan, Z.-A.; Wu, M.; Fang, Z.; Zhang, Y.; Chen, X.; Zhang, G.; Wang, X. Ionothermal Synthesis of Covalent Triazine Frameworks in a NaCl-KCl-ZnCl2 Eutectic Salt for the Hydrogen Evolution Reaction. *Angewandte Chemie International Edition* **2022**, *61* (18), No. e202201482.
(24) Hu, F.; Zhang, T.; Wang, J.; Li, S.; Liu, C.; Song, C.; Shao, W.; Liu, S.; Jian, X. Constructing N, O-Containing micro/mesoporous covalent triazine-based frameworks toward a detailed analysis of the combined effect of N, O heteroatoms on electrochemical performance. *Nano Energy* **2020**, *74*, No. 104789.
(25) Ball, B.; Chakravarty, C.; Sarkar, P. Silicon and Phosphorus Co-doped Bipyridine-Linked Covalent Triazine Framework as a Promising Metal-Free Catalyst for Hydrogen Evolution Reaction: A Theoretical Investigation. *The Journal of Physical Chemistry Letters* **2020**, *11* (4), 1542−1549.
(26) Krishnaraj, C.; Jena, H. S.; Leus, K.; Van Der Voort, P. Covalent triazine frameworks − a sustainable perspective. *Green Chemistry* **2020**, *22* (4), 1038−1071.
(27) Liu, M.; Huang, Q.; Wang, S.; Li, Z.; Li, B.; Jin, S.; Tan, B. Crystalline Covalent Triazine Frameworks by In Situ Oxidation of Alcohols to Aldehyde Monomers. *Angew. Chem.* **2018**, *130* (37), 12144−12148.
(28) Yu, S. Y.; Mahmood, J.; Noh, H. J.; Seo, J. M.; Jung, S. M.; Shin, S. H.; Im, Y. K.; Jeon, I. Y.; Baek, J. B. Direct Synthesis of a Covalent Triazine-Based Framework from Aromatic Amides. *Angew. Chem., Int. Ed.* **2018**, *57*, 8438.
(29) Wang, K.; Yang, L. M.; Wang, X.; Guo, L.; Cheng, G.; Zhang, C.; Jin, S.; Tan, B.; Cooper, A. Covalent Triazine Frameworks via a Low-Temperature Polycondensation Approach. *Angewandte Chemie International Edition* **2017**, *56* (45), 14149−14153.
(30) Ren, S.; Bojdys, M. J.; Dawson, R.; Laybourn, A.; Khimyak, Y. Z.; Adams, D. J.; Cooper, A. I. Porous, Fluorescent, Covalent Triazine-Based Frameworks Via Room-Temperature and Microwave-Assisted Synthesis. *Adv. Mater.* **2012**, *24* (17), 2357−2361.
(31) Kuhn, P.; Antonietti, M.; Thomas, A. Porous, covalent triazine-based frameworks prepared by ionothermal synthesis. *Angewandte chemie international edition* **2008**, *47* (18), 3450−3453.
(32) Jena, H. S.; Krishnaraj, C.; Schmidt, J.; Leus, K.; Van Hecke, K.; Van Der Voort, P. Effect of Building Block Transformation in Covalent Triazine-Based Frameworks for Enhanced CO_2 Uptake and Metal-Free Heterogeneous Catalysis. *Chem. − Eur. J.* **2020**, *26* (7), 1548−1557.
(33) Jena, H. S.; Krishnaraj, C.; Wang, G.; Leus, K.; Schmidt, J.; Chaoui, N.; Van Der Voort, P. Acetyl Acetone Covalent Triazine Framework: An Efficient Carbon Capture and Storage Material and a Highly Stable Heterogeneous Catalyst. *Chem. Mater.* **2018**, *30* (12), 4102−4111.
(34) Rangaraj, V. M.; Reddy, K. S. K.; Karanikolos, G. N. Ionothermal synthesis of phosphonitrilic-core covalent triazine frameworks for carbon dioxide capture. *Chemical Engineering Journal* **2022**, *429*, No. 132160.
(35) Krishnaraj, C.; Jena, H. S.; Leus, K.; Freeman, Helen M.; Benning, L. G.; Van Der Voort, P. An aliphatic hexene-covalent triazine framework for selective acetylene/methane and ethylene/methane separation. *J. Mater. Chem. A* **2019**, *7* (21), 13188−13196.

https://doi.org/10.1021/acsanm.3c03248
ACS Appl. Nano Mater. XXXX, XXX, XXX−XXX

(36) Wang, G.; Leus, K.; Jena, H. S.; Krishnaraj, C.; Zhao, S.; Depauw, H.; Tahir, N.; Liu, Y.-Y.; Van Der Voort, P. A fluorine-containing hydrophobic covalent triazine framework with excellent selective CO 2 capture performance. *Journal of Materials Chemistry A* **2018**, *6* (15), 6370−6375.
(37) Gunasekar, G. H.; Park, K.; Ganesan, V.; Lee, K.; Kim, N.-K.; Jung, K.-D.; Yoon, S. A Covalent Triazine Framework, Functionalized with Ir/N-Heterocyclic Carbene Sites, for the Efficient Hydrogenation of CO2 to Formate. *Chem. Mater.* **2017**, *29* (16), 6740−6748.
(38) Tahir, N.; Wang, G.; Onyshchenko, I.; De Geyter, N.; Leus, K.; Morent, R.; Van Der Voort, P. High-nitrogen containing covalent triazine frameworks as basic catalytic support for the Cu-catalyzed Henry reaction. *J. Catal.* **2019**, *375*, 242−248.
(39) Tahir, N.; Muniz-Miranda, F.; Everaert, J.; Tack, P.; Heugebaert, T.; Leus, K.; Vincze, L.; Stevens, C. V.; Van Speybroeck, V.; Van Der Voort, P. Immobilization of Ir(I) complex on covalent triazine frameworks for CH borylation reactions: A combined experimental and computational study. *J. Catal.* **2019**, *371*, 135−143.
(40) Guo, L.; Niu, Y.; Razzaque, S.; Tan, B.; Jin, S. Design of D−A1−A2 Covalent Triazine Frameworks via Copolymerization for Photocatalytic Hydrogen Evolution. *ACS Catalysis* **2019**, *9* (10), 9438−9445.
(41) Guo, L.; Niu, Y.; Xu, H.; Li, Q.; Razzaque, S.; Huang, Q.; Jin, S.; Tan, B. Engineering heteroatoms with atomic precision in donor−acceptor covalent triazine frameworks to boost photocatalytic hydrogen production. *Journal of Materials Chemistry A* **2018**, *6* (40), 19775−19781.
(42) Lan, X.; Liu, X.; Zhang, Y.; Li, Q.; Wang, J.; Zhang, Q.; Bai, G. Unveiling Charge Dynamics in Acetylene-Bridged Donor−π−Acceptor Covalent Triazine Framework for Enhanced Photoredox Catalysis. *ACS Catalysis* **2021**, *11* (12), 7429−7441.
(43) Jena, H. S.; Krishnaraj, C.; Parwaiz, S.; Lecoeuvre, F.; Schmidt, J.; Pradhan, D.; Van Der Voort, P. Illustrating the Role of Quaternary-N of BINOL Covalent Triazine-Based Frameworks in Oxygen Reduction and Hydrogen Evolution Reactions. *ACS Applied Materials & Interfaces* **2020**, *12* (40), 44689−44699.
(44) Qu, K.; Zheng, Y.; Jiao, Y.; Zhang, X.; Dai, S.; Qiao, S.-Z. Polydopamine-Inspired, Dual Heteroatom-Doped Carbon Nanotubes for Highly Efficient Overall Water Splitting. *Adv. Energy Mater.* **2017**, *7* (9), No. 1602068.
(45) Asefa, T. Metal-Free and Noble Metal-Free Heteroatom-Doped Nanostructured Carbons as Prospective Sustainable Electrocatalysts. *Acc. Chem. Res.* **2016**, *49* (9), 1873−1883.
(46) Liu, M.; Yang, K.; Li, Z.; Fan, E.; Fu, H.; Zhang, L.; Zhang, Y.; Zheng, Z. The O/S heteroatom effects of covalent triazine frameworks for photocatalytic hydrogen evolution. *Chemical Communications* **2021**, *58* (1), 92−95.
(47) Meier, C. B.; Clowes, R.; Berardo, E.; Jelfs, K. E.; Zwijnenburg, M. A.; Sprick, R. S.; Cooper, A. I. Structurally Diverse Covalent Triazine-Based Framework Materials for Photocatalytic Hydrogen Evolution from Water. *Chem. Mater.* **2019**, *31* (21), 8830−8838.
(48) Huang, W.; He, Q.; Hu, Y.; Li, Y. Molecular Heterostructures of Covalent Triazine Frameworks for Enhanced Photocatalytic Hydrogen Production. *Angewandte Chemie International Edition* **2019**, *58* (26), 8676−8680.
(49) Chapter 8 - Phosphorus Compounds. In *Interpreting Infrared, Raman, and Nuclear Magnetic Resonance Spectra*; Nyquist, R. A., Ed.; Academic Press: San Diego, 2001; pp 231-350.
(50) Xu, Y.-T.; Liu, S.-Z.; Li, D.; Tian, S.-C.; Qiu, J.-J.; Liu, C.-M. Synthesis of Hexakis-(4-tetrazolylphenyloxy)cyclotriphosphazene and Its Alkylonitrile Derivative. *Synth. Commun.* **2011**, *41* (9), 1370−1375.
(51) Yan, B.; Yang, G. Enhancing electron density of bulk g-C3N4 through phosphorus doping for promoting photocatalytic hydrogen evolution reaction. *Appl. Surf. Sci.* **2021**, *570*, No. 151186.
(52) Osadchii, D. Y.; Olivos-Suarez, A. I.; Bavykina, A. V.; Gascon, J. Revisiting nitrogen species in covalent triazine frameworks. *Langmuir* **2017**, *33* (50), 14278−14285.
(53) Bhunia, S.; Das, S. K.; Jana, R.; Peter, S. C.; Bhattacharya, S.; Addicoat, M.; Bhaumik, A.; Pradhan, A. Electrochemical Stimuli-Driven Facile Metal-Free Hydrogen Evolution from Pyrene-Porphyrin-Based Crystalline Covalent Organic Framework. *ACS Applied Materials & Interfaces* **2017**, *9* (28), 23843−23851.
(54) Patra, B. C.; Khilari, S.; Manna, R. N.; Mondal, S.; Pradhan, D.; Pradhan, A.; Bhaumik, A. A Metal-Free Covalent Organic Polymer for Electrocatalytic Hydrogen Evolution. *ACS Catalysis* **2017**, *7* (9), 6120−6127.
(55) DOI: 10.1039/C6TA05863A. Yan, D.; Dou, S.; Tao, L.; Liu, Z.; Liu, Z.; Huo, J.; Wang, S. Electropolymerized supermolecule derived N, P co-doped carbon nanofiber networks as a highly efficient metal-free electrocatalyst for the hydrogen evolution reaction. *Journal of Materials Chemistry A* **2016**, *4* (36), 13726−13730.
(56) Talapaneni, S. N.; Kim, J.; Je, S. H.; Buyukcakir, O.; Oh, J.; Coskun, A. Bottom-up synthesis of fully sp2 hybridized three-dimensional microporous graphitic frameworks as metal-free catalysts. *Journal of Materials Chemistry A* **2017**, *5* (24), 12080−12085.
(57) Shinde, S. S.; Sami, A.; Lee, J.-H. Electrocatalytic hydrogen evolution using graphitic carbon nitride coupled with nanoporous graphene co-doped by S and Se. *Journal of Materials Chemistry A* **2015**, *3* (24), 12810−12819.
(58) Shinde, S. S.; Sami, A.; Lee, J.-H. Nitrogen- and Phosphorus-Doped Nanoporous Graphene/Graphitic Carbon Nitride Hybrids as Efficient Electrocatalysts for Hydrogen Evolution. *ChemCatChem* **2015**, *7* (23), 3873−3880.
(59) Ito, Y.; Cong, W.; Fujita, T.; Tang, Z.; Chen, M. High Catalytic Activity of Nitrogen and Sulfur Co-Doped Nanoporous Graphene in the Hydrogen Evolution Reaction. *Angewandte Chemie International Edition* **2015**, *54* (7), 2131−2136.
(60) Zhu, J. W.; Mu, S. C. Defect Engineering in the Carbon-Based Electrocatalysts: Insight into the Intrinsic Carbon Defects. *Adv. Funct. Mater.* **2020**, *30*, No. 2001097.
(61) Perdew, J. P.; Burke, K.; Ernzerhof, M. Generalized Gradient Approximation Made Simple. *Phys. Rev. Lett.* **1996**, *77* (18), 3865.
(62) Grimme, S.; Antony, J.; Ehrlich, S.; Krieg, H. A Consistent and Accurate Ab Initio Parametrization of Density Functional Dispersion Correction (DFT-D) for the 94 Elements H-Pu. *J. Chem. Phys.* **2010**, *132* (15), 154104.
(63) Grimme, S.; Ehrlich, S.; Goerigk, L. Effect of the Damping Function in Dispersion Corrected Density Functional Theory. *J. Comput. Chem.* **2011**, *32* (7), 1456−1465.
(64) Kresse, G.; Furthmüller, J. Efficiency of Ab-Initio Total Energy Calculations for Metals and Semiconductors Using a Plane-Wave Basis Set. *Comput. Mater. Sci.* **1996**, *6* (1), 15−50.
(65) Kresse, G.; Joubert, D. From Ultrasoft Pseudopotentials to the Projector Augmented-Wave Method. *Phys Rev B* **1999**, *59* (3), 1758.
(66) Nørskov, J. K.; Rossmeisl, J.; Logadottir, A.; Lindqvist, L.; Kitchin, J. R.; Bligaard, T.; Jónsson, H. Origin of the Overpotential for Oxygen Reduction at a Fuel-Cell Cathode. *J. Phys. Chem. B* **2004**, *108* (46), 17886−17892.

https://doi.org/10.1021/acsanm.3c03248
ACS Appl. Nano Mater. XXXX, XXX, XXX−XXX